Geology, Geophysics & Environment 2024, vol. 50 (3): 253–274

Complex and spatial analysis of geophysical data recorded in the areas of karst forms developed in horst structures

Tomisław Gołębiowski[1], Michał Ćwiklik[2], Dominika Guzior[3]

[1] *Cracow University of Technology, Faculty of Environmental Engineering and Energy, Krakow, Poland, e-mail: tomislaw.golebiowski@pk.edu.pl (corresponding author), ORCID ID: 0000-0002-4005-2265*
[2] *Cracow University of Technology, Faculty of Environmental Engineering and Energy, Krakow, Poland, ORCID ID: 0000-0002-3206-2877*
[3] *Cracow University of Technology, Faculty of Environmental Engineering and Energy, Krakow, Poland*

Received: 26 May 2024; accepted: 12 July 2024; first published online: 30 September 2024

Abstract: The paper presents the results of geophysical surveys carried out over two voids occurring in limestone in the area of the Zakrzówek horst in Krakow, Poland. The first void was an anthropogenic cavern in the Kostrze site (a district of Krakow), while the second one was the Jasna cave (located in a reserve named "The Twardowski Rocks"). The main terrain surveys were carried out using GPR (ground penetrating radar). To reduce interpretative ambiguity, the GPR results were correlated with additional results obtained from two other methods, i.e. the GCM (ground conductivity meter) and ERT (electrical resistivity tomography). The main aim of the geophysical surveys was the detection and 3D visualisation of karst forms developed around both voids located in horst structures in limestone. The particular purpose of the research was to try to clarify the geological nature of the GPR anomalies characterised by an almost complete lack of reflections; both ohmic and scattering attenuations of GPR signals were analysed to solve the reduction of the reflection amplitudes. Another important fact discussed in the paper was the low consistency and similarity of the results obtained from geophysical surveys carried out above the Jasna cave. The interpretation of the GPR and GCM data recorded over the anthropogenic cavern allowed the places of strong weathering/fracturing of limestone to be indicated as well as a zone of limestone filled with clay-rich material. The interpretation of the GPR and ERT data recorded over the cave made it possible to identify areas of the strong weathering/fracturing of limestone, faults, anastomoses and karst chimneys.

Keywords: GPR, GCM, ERT, karst forms, horst structure

INTRODUCTION

The non-invasive geophysical examination of karst forms using different geophysical methods has been applied with success for many years. In this paper, the authors focus on the geophysical investigation of karst forms developed in horst structures in limestone with the use of selected electrical and electromagnetic methods. The main terrain surveys were carried out using the GPR method which is one of the electromagnetic techniques characterised by a very high resolution of its measurements. To reduce interpretative ambiguity, the GPR results were correlated with additional results obtained from the GCM method, another electromagnetic technique, and the ERT method which is an electrical technique.

All of the listed methods are well known in geophysics and thus they have not been described in the paper; detailed information concerning the GPR, ERT and GCM techniques may be found in the geophysical literature, e.g. Reynolds (2011), Everett (2013). The application of geophysical electrical and electromagnetic methods for the detection of karst forms and the monitoring of karst phenomena in limestone has been utilised by many geophysicists.

Maślakowski et al. (2024) employed the ERT method to diagnose karst in road engineering in Lublin Upland. The method facilitated the indication of zones of the possible occurrence of karst or erosional incisions in carbonate rocks, including potential karst voids or incisions filled with Quaternary sediments, predominantly sandy or clay-rich weathering residues. Verdet et al. (2020) applied the ERT technique to detect undercover karst features in the Lascaux cave hill (France). Geophysical measurements have been used to define the boundary between exposed Coniacian or Santonian limestone formations and clay-rich sand deposits. Stan-Kłeczek et al. (2020) presented the use of the ERT method to identify underground karst structures at two locations in the Silesian region in Poland. Similarly, in her article Pasierb (2022) describes the application of 2D/3D ERT surveys in studying the limestone karst of the Zakrzówek Horst.

Łyskowski et al. (2014) employed the GPR method for the investigation of limestone karst at the Odstrzelona cave in the village of Kowala (Świętokrzyskie Mountains, Poland). The GPR surveys revealed the presence of two extra chambers and several additional openings within the limestone. In their article, Zieliński et al. (2016) presented GPR mapping of karst formations under a historic building in the town of Szydłów, Poland. The findings validated the presence of previously undiscovered voids and areas of weathering within the rock structure. In his paper, Ortyl (2019) explored the potential for mapping karst features using the GPR method.

Combined geophysical investigations have frequently been carried out for analysis purposes. For instance, in their article, Margiotta et al. (2015) explained how karst phenomena are recognised and monitored in the Saleto area in Apulia, southeastern Italy, using the GPR and ERT methods. Similarly, Artugyan et al. (2020) presented the process and application of GPR and ERT surveys as complementary methods in studying karst phenomena in the Cuptoare cave and Buhui cave in Romania, in the Anina region. In their geophysical and geological investigations in Salice Salentino in Italy, Leucci et al. (2004) used the GPR and ERT methods for mapping karstic cavities or karstified zones.

There is no doubt that the GPR and ERT methods are at the forefront of the geophysical examination of karst forms but some issues remain, In order to solve some of the problems, other geophysical methods may also be applied. For example, Bozzo et al. (1996) presented an article in which they discussed the application of different geophysical methods, i.e. VLF (very low frequency), refraction seismic, gravity and magnetic methods to study near-surface karst structures (dolines) in Ligurian Alps in Italy. Armadillo et al. (1998) surveyed the doline of S. Pietro dei Monti (Western Liguria, Italy) using the magnetic and VLF methods. In their study, Martínez-Moreno et al. (2014) compared and contrasted the results of different geophysical methods, i.e. ERT, GPR, IP, MP, 2D seismic prospection, in order to describe the karst system surrounding the Gruta de las Maravillas cave (Aracena, Spain). Kasprzak et al. (2015) presented surface GPR and ERT surveys and LiDAR DTM analysis combined with underground cave mapping for karst system exploration in the Niedźwiedzia cave in the area of the Kleśnica Valley (the Sudetes, Poland). It represented a comprehensive approach focused on investigating the distribution of karst voids within the Kleśnica Valley. Through the comparison and analysis of spatial data obtained from different measurement techniques, it was possible to delineate the boundaries of crystalline limestone formations and identify the distribution of karst voids, including those previously unidentified and unexplored.

The first aim of the geophysical surveys presented in the paper was the detection and 3D visualisation of karst forms which have developed around anthropogenic or natural voids located

in horst structures in limestone. Both voids were known, accessible, and were measured thoroughly, and they were treated as an indicator that other karst forms may occur in the investigation sites. The second aim of the research was the analysis of the geophysical data recorded around both voids – the authors tried to clarify the geological nature of the GPR anomalies appearing at both sites, characterised by strong reduction of signal amplitudes; the scattering attenuation of GPR signals in weathered/fractured limestone was also analysed. Another important fact discussed in the paper was the low consistency and similarity of the results obtained from geophysical surveys carried out over a natural void.

LOCATION OF STUDIED AREAS

Non-invasive geophysical surveys were carried out in the area of the Zakrzówek horst, in Krakow, Poland (Fig. 1) over the anthropogenic cavern known as "the cavern under the chapel" (the Kostrze district of Krakow) and over a natural void called the Jasna cave.

During the Austrian partition era in the village of Kostrze, a defensive structure called "Fort No 53" or "Fort Bodzów" was built. During World War I, several caverns were hollowed out in the limestone rocks surrounding this fort, forming interconnected corridors serving various functions. The geophysical surveys were carried out in the area of the anthropogenic cavern known as "the cavern under the chapel" (Fig. 2) which was likely constructed around 1915–1916 as one of the elements of "Fort No 53". Analysing the shape of this cavern (Fig. 2B), it is likely that it was a natural void which was adapted and extended by Austrian soldiers for storage purposes. We have chosen this object for research to check whether anthropogenic activity caused the creation of additional fractures around the cavern. Positioned above the cavern is a chapel dating from the turn of the 19th and 20th centuries. The total length of the cavern is 100 m and it can be accessed through three entrances (Fig. 2B). The main entrance is located on the southern side of the examined area. Two additional entrances are located in its northern part, where collapsed ceilings pose a danger. The cavern consists of a single large storage chamber (Fig. 4A) and corridors leading to it. The main chamber extends into a tunnel, which apparently led to another entrance from the southwest, but this was closed off due to a collapsed ceiling.

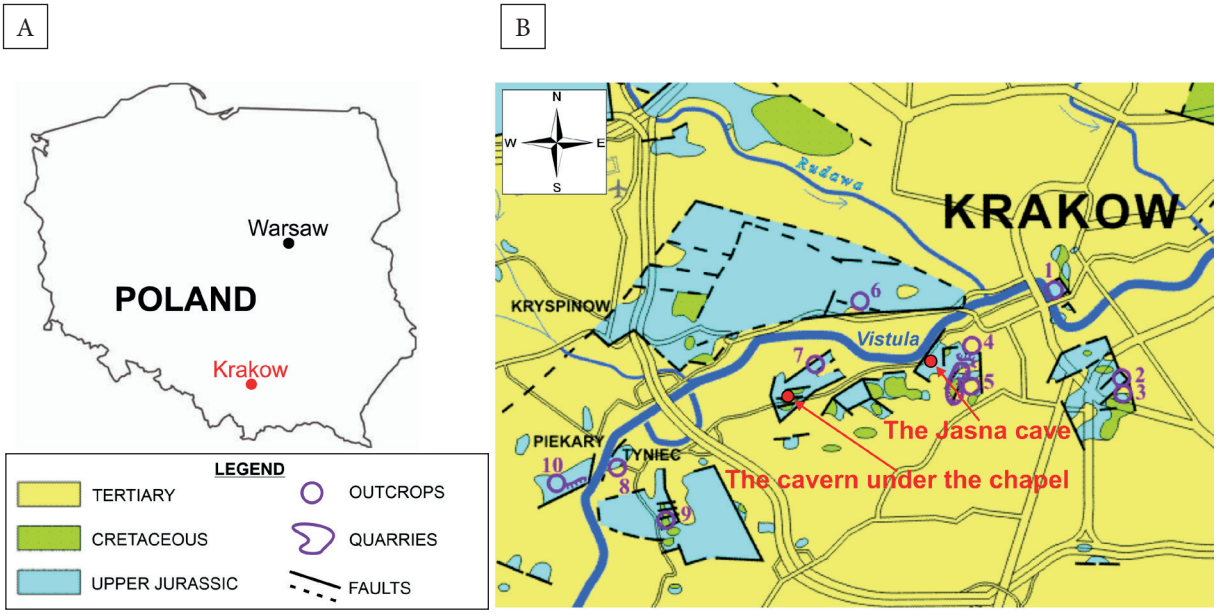

Fig. 1. *Location of the geophysical investigation sites (A); geological information from the investigation sites – map without Quaternary deposits (www.ing.pan.pl/muzeum-geologiczne/tytul-domyslny – modified) (B)*

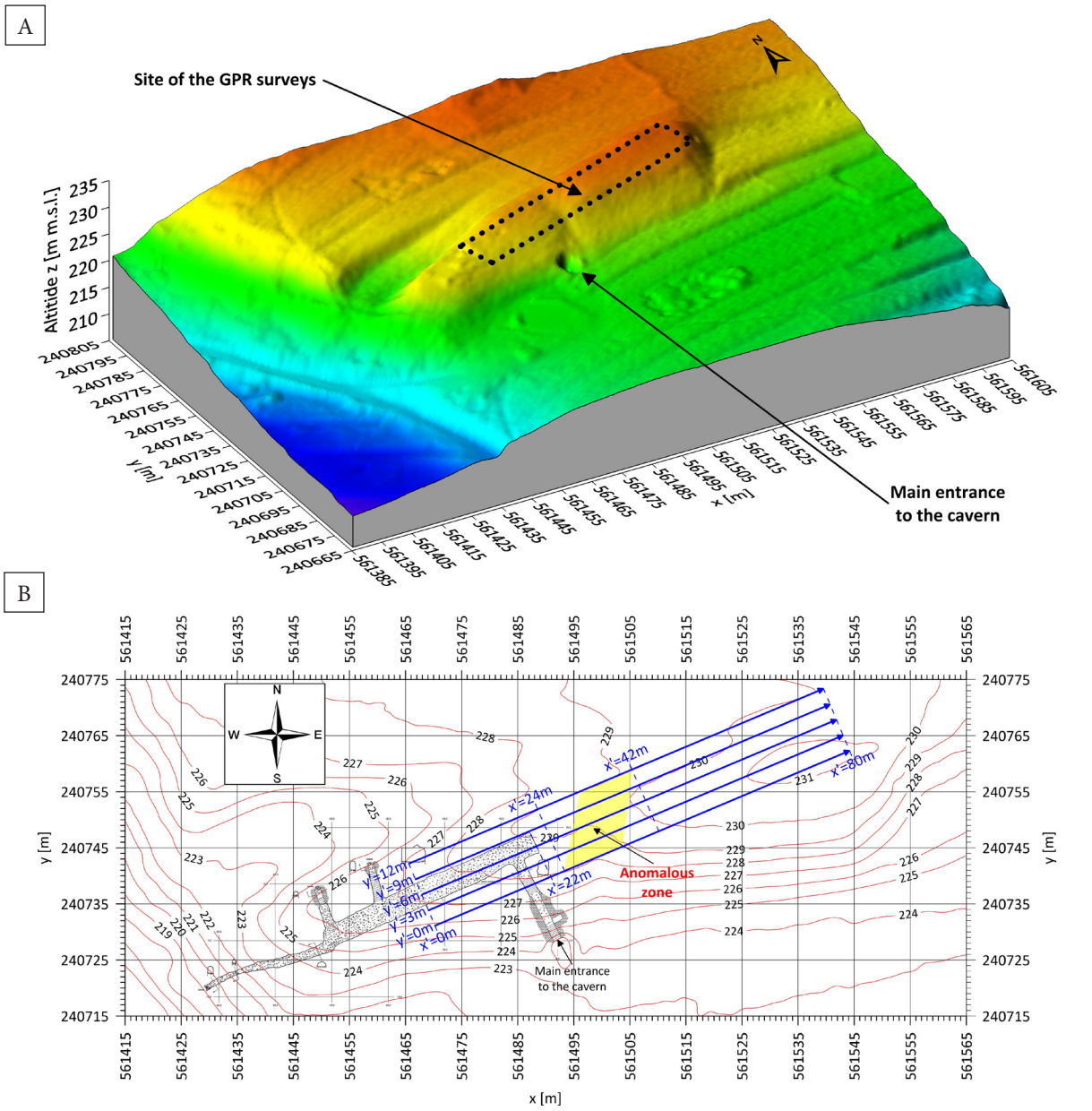

Fig. 2. *Investigation site called "The cavern under the chapel": A) numerical terrain model (prepared in the Surfer program on the basis of data from https://mapy.geoportal.gov.pl); B) project of geophysical profiles (prepared in the Surfer program on the basis of data from https://mapy.geoportal.gov.pl and http://kaponiera.pl/8/kawernapodkapliczka.html)*

The studied area around the Jasna cave is characterised by a distinctive landscape as it is situated in the zone of structural ridges. One such ridge is the Zakrzówek horst (Fig. 1B – a region of quarry and outcrops no. 4 and 5) which was formed during the Paleogene era by the geological upheavals of the Alpine movements. Within the ridge area, a nature reserve called "Twardowski's Rocks" was established and several karst caves and inactive quarries are located there. This tectonic structure is marked by uplifts and fault lines – the primary faults trend in the southwest to the northeast and the northwest to the southeast direction, with vertical shifts of approximately 200 m. The central part of the ridge is composed primarily of densely packed Upper Jurassic limestone, with an estimated thickness of 225 m. In certain areas, deposits of Cretaceous formations can be found, including marls and marly limestones (Fig. 3A).

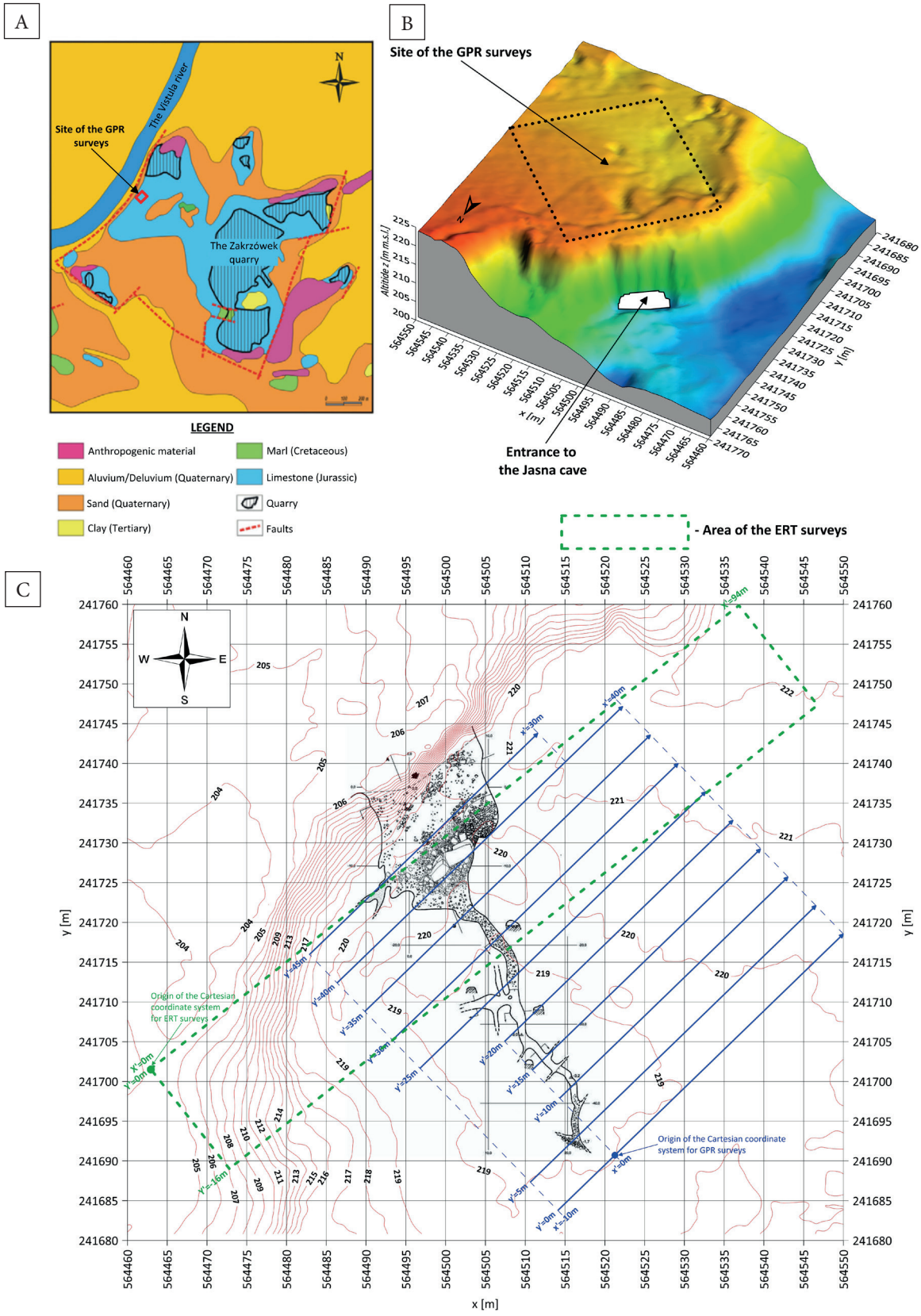

Fig. 3. *Investigation site called "The Jasna cave": A) geological settings in the Zakrzówek horst (Motyka et al. 2003); B) numerical terrain model (prepared in the Surfer program on the basis of data from https://mapy.geoportal.gov.pl); C) project of geophysical profiles (prepared in the Surfer program on the basis of data from https://mapy.geoportal.gov.pl and https://jaskiniepolski.pgi.gov.pl/Details/Information/2082)*

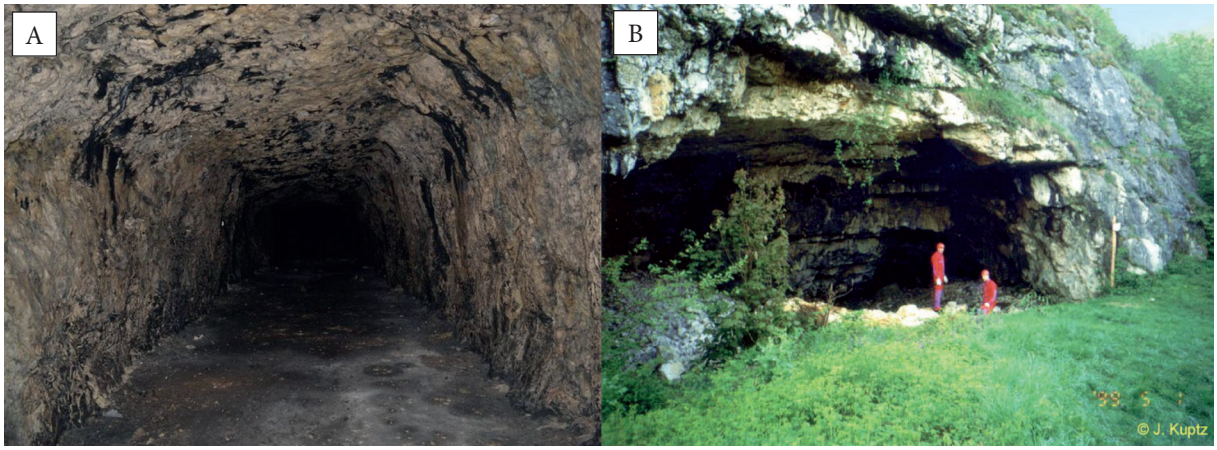

Fig. 4. *The main chamber of "The cavern under the chapel" (http://kaponiera.pl/8/kawernapodkapliczka.html) (A); the entrance and the main chamber of the Jasna cave (http://www.sktj.pl/epimenides/jura/jaswis_p.html) (B)*

The tectonic troughs that separate the ridges are filled with Miocene sediments and overlaid with Quaternary sediments. Around the Zakrzówek horst, there are also formations of anthropogenic origin, especially on the eastern side of the former quarry (Fig. 3A). Among the Quaternary formations, there are alluvial deposits closely linked to the Vistula River through hydraulic connections (Fig. 3A). Caves represent a significant natural feature of the Zakrzówek horst, with the Jasna cave (where geophysical surveys were carried out – Fig. 3B, C) being the second largest cave within the studied area. Situated in the northwestern part of the ridge, and in close proximity to the Vistula River, the cave boasts an entrance approximately 5 m high and 15 m wide (Figs. 3C, 4B). Beyond the entrance, there is a spacious chamber, its floor scattered with large boulders. The floor of the cave gradually descends, and towards the rear, the chamber transitions into a narrow corridor, which takes a southeastern direction. This corridor extends for 35 m, with its initial section also cluttered with detached rocks. Approximately halfway along the length of the passage, other corridors branch off from it. In the initial section, the corridors are narrow and tight, further transitioning into crevices that cannot be traversed. At the end of the main corridor there are also detached rocks.

GEOPHYSICAL METHODS AND TERRAIN SURVEY PROJECTS

In both sites, GPR surveys with the application of the short-offset reflection profiling technique were carried out with the use of the Swedish Pro-Ex GPR system (www.guidelinegeo.com). Acquisition parameters assumed during the terrain surveys were presented in Table 1.

Local Cartesian x'-y'-z systems were established in both investigation sites and subsequently parallel profiles with a constant distance between them $\Delta y' = 3$ m (over the cavern under the chapel – Fig. 2B) and $\Delta y' = 5$ m (over the Jasna cave – Fig. 3C) were designed.

Table 1
GPR acquisition parameters

Site	Antenna frequency [MHz]	Mean resolution [m]	Max. depth range (in lossless media) [m]	Interval between traces [m]	Stacking (to improve signal/noise ratio) [number of times]
The cavern under the chapel	250	0.10	15	0.05	32
The Jasna cave	100	0.25	30	0.10	32

Before starting the detailed GPR measurements, several reconnaissance profiles with different orientations were designed over the cavern. The analysis of the results from reconnaissance profiles delivered information about the presence of an anomalous zone (Fig. 2B), analysed in the paper; parallel profiles were designed more-less perpendicularly to the anomalous zone.

GPR investigations over the Jasna cave were carried out in several measurement sessions, in the period between 2009 and 2012, with the application of different antennae, i.e. 100–250–500 MHz. The selected results from those surveys were presented in a thus far unpublished Engineering Thesis (Parczeński 2012, Trybuch 2024). In the paper, results obtained from 100 MHz antennae were presented and discussed.

For raw GPR data recorded at both sites, standard processing procedures were applied, i.e.: DC shift, dewow, background removal, median filter, Butterworth filter, gain function and static correction. A detailed description of applied procedures may be found in Annan (1999, 2001), ReflexW Manual (2023). For the processing and visualisation of GPR data, ReflexW software (www.sandmeier-geo.de) was applied.

For the time-depth conversion of radargrams, a mean velocity of 0.12 m/ns, typical for limestone, was assumed. All radargrams were presented in normalised scale with normalisation of signals amplitudes to max. amplitude of the direct air wave.

Supplementary GCM surveys over the cavern (Fig. 2B) were conducted along the same five profiles as GPR surveys. The measurements were carried out with intervals of Δx = 1 m which resulted in the spatial resolution being significantly lower than during GPR measurements (Table 1 – intervals Δx = 0.05 m). CMD-Explorer conductivity meter, manufactured by GF Instruments (www.gfinstruments.cz), was used as measuring device. Due to the larger depth of the investigation, the coils with the vertical orientation (VD) and 10 kHz frequency were used. The apparent conductivity σ_a (mS/m) of the investigated geological medium at depths 2.2 m, 4.2 m and 6.7 m was measured. The field data were inverted using Res2DInv software (www.aarhusgeosoftware.dk). A robust inversion method was employed to achieve a clearer and sharper boundary between different zones with varying resistivity values (Loke 2011), which was expected based on the GPR data. Additionally, the robust inversion method brings the lowest absolute Root Mean Square value, which never exceeded 5% in any instance. A topographic correction was taken into account in the inversion process (Turarova et al. 2022).

To reduce interpretation ambiguity, the results of GPR surveys over the cave (Fig. 3C) were correlated with the results of ERT surveys presented in the paper by Pasierb (2022). The ERT measurements were carried out along five parallel profiles with 4 m distances between them; 94-metre-long profiles were designed near the main chamber of the Jasna cave (Fig. 3C). The ERT profiles were rotated at a slightly different angle to the GPR profiles (Fig. 3C), so new local Cartesian system, described with upper case letters X' and Y', was established. The terrain surveys were carried out using ARES system manufactured by GF Instruments (www.gfinstruments.cz) and the roll-along technique with the dipole-dipole array were used for data acquisition. The ERT measurements were performed with electrode spacing Δx = 2 m, lengths of current and potential dipoles was a = 1, 3, 5, 7, 9Δx, whereas the separation rate, being the ratio of the distances between a current dipole and a potential dipole was equal to n = 1, 2, 3, 4. The measurement error was assumed at a level of 2%, which mean that observations with a standard deviation error of more than 2% were repeated or discarded.

The 2D inversion process, with the use of Res2DInv software (www.aarhusgeosoftware.dk), was carried out using the robust data constraint option. The files in the 2D format were converted into one data file in the format used in the 3D inversion process, and for the 3D inversion, Res3DInv software (www.aarhusgeosoftware.dk) was applied.

Additionally, for the GCM and ERT data visualisation, Surfer and Voxler software (www.goldensoftware.com) were used.

RESULTS AND DISCUSSION

"The cavern under the chapel" Investigation site

In Figure 5, 3D volumetric visualisation of the main anomalies over the cavern is presented. For this type of visualisation, amplitudes between several profiles were interpolated in the y' direction; afterwards, amplitudes were converted into the envelopes using the Hilbert transform; in the last step, amplitude threshold was applied, meaning only amplitudes higher than 50% of max. amplitude were shown. Additionally, a shading procedure was applied for the better visualisation of several anomalies.

In Figure 5, highly weathered/fractured limestone is evident to the depth of ca. 10 m. In the initial parts of some of the profiles, reflections from the top of the cavern were recorded. The most interesting anomaly in Figure 5 is a zone with a high reduction of reflection amplitudes in the central part of the examined area. Generally, a lack of reflections in a radargram may be caused by:

- lack of reflector in the geological medium,
- presence of reflector but low value of reflection coefficient,
- presence of reflector but high ohmic attenuation of examined medium,
- presence of reflector but high scattering attenuation of examined medium.

The last point, i.e. a scattering attenuation was relatively seldom analysed in papers connected with the GPR method. A scattering attenuation often occurs in regions subjected to antropopression, e.g. mining regions or highly urbanised areas (Gołębiowski 2023). The problem of the detection of voids under the near-surface weathered/fractured zone which causes a scattering attenuation was analysed in publications by Gołębiowski (2010, 2012). Despite the presence of a near-surface weathered/fractured zone (Fig. 5), scattering attenuation does not play a significant role in this site since readable reflections from the top of the cavern were recorded.

It may be assumed that only boundaries with a high reflection coefficient occur in this site, i.e. soil and limestone, limestone and cavern, limestone and dry or water saturated rock with higher porosity (near-surface weathered/fractured zone). So, the second point above may be omitted in further analysis.

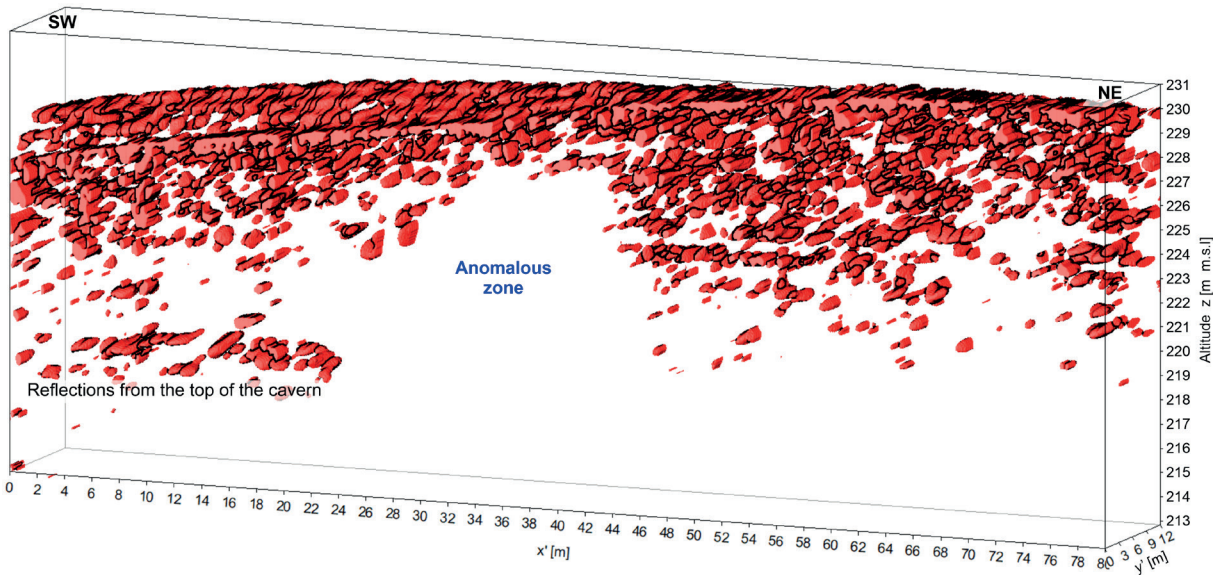

Fig. 5. *3D volumetric visualisation of the main GPR anomalies*

In the analysed situation, a lack of reflections in the anomalous zone may be the result of either an existing of solid block of limestone and accompanying lack of reflectors in the form of fractures (the first point above) or the presence of geological material with high ohmic attenuation (the third point above), e.g. highly weathered/fractured limestone with free spaces colmatated with clay.

A block of solid limestone might have appeared in this area due to tectonic processes and the presence of local faults (Fig. 1B). The aforementioned colmatation process may be a result of washing out from the slope (Fig. 2A) the Tertiary and Quaternary deposits. To verify which hypothesis is true, additional surveys with the application of the GCM method were performed.

For the better visualisation and measuring of an anomalous zone seen in Figure 5, depth slice and several x' cuts of 3D block were prepared (Fig. 6). Figure 6 was constructed by interpolation of information in the y' direction and signal amplitudes were transformed into envelopes with the use of the Hilbert transform.

The direction of the spread of the anomalous zone from S to N is clearly visible in Figure 6A which presents a depth slice at z = 224 m (depth d = 7 m). In Figure 6B, four x' cuts through an anomalous zone are presented; it may be noticed that an anomalous zone spreads vertically almost from the earth surface to the depth of over 10 m (Fig. 6B).

For the easier measurement of the anomalous zone in x'-z plane, y' cuts of 3D block (Fig. 5) were made and presented in Figure 7, in a typical form, i.e. as signal amplitudes distribution. In all y' cuts (Fig. 7), the stochastically distributed reflections from highly weathered/fractured limestone are visible; reflections from the top of the cavern are also evident. In Figure 7, an anomalous zone spreads between x' = 24 m and x' = 35 m, at y' = 0 m and x' = 32 m and x' = 42 m, at y' = 12 m.

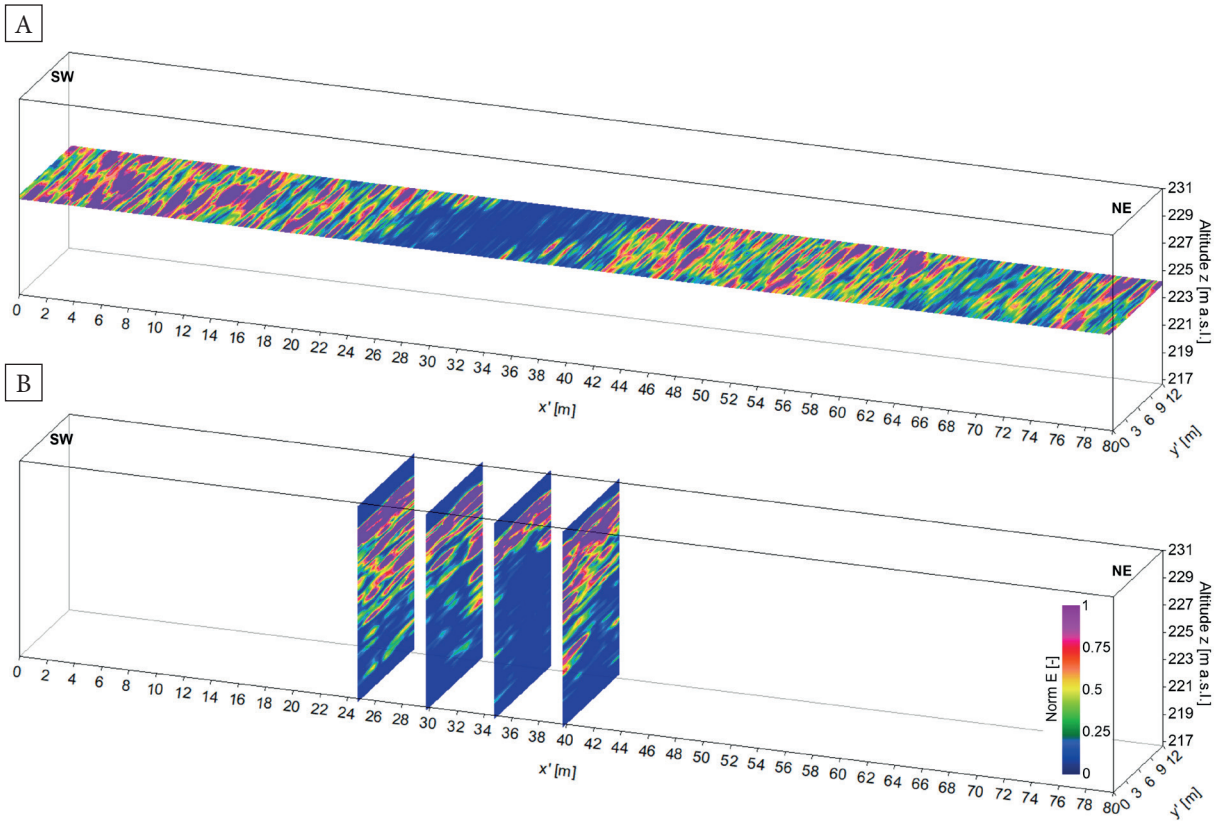

Fig. 6. *GPR results in form of several cuts: A) depth slice of 3D block (Fig. 5) at depth d = 7 m, altitude z = 224 m; B) x' cuts of anomalous zone with step Δx' = 5 m*

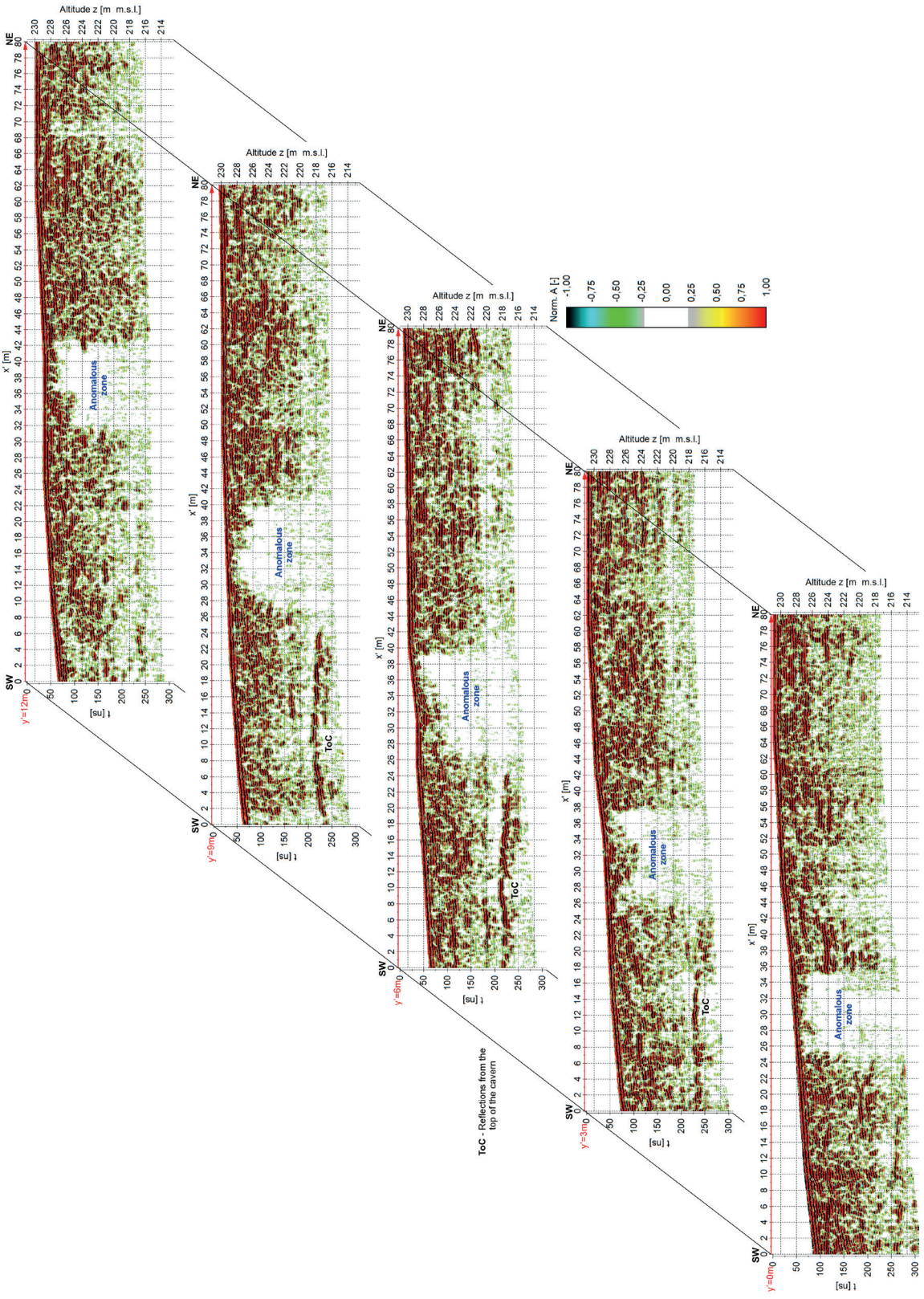

Fig. 7. GPR results in form of y' cuts of 3D block (Fig. 5) with step Δy' = 3 m

Similarly to the GPR method, the 3D visualisation of the main anomalies in the form of resistivity distribution was prepared first (Fig. 8). For the better visualisation of several anomalies, values of resistivity below 800 Ωm were removed from the figure by applying an adequate level of transparency. In Figure 8, a low resistivity zone, located in the same position as the anomalous zone in the GPR results, is clearly visible. Such a GCM anomaly delivers information that an anomalous zone in this area is caused by the presence of a mixture made of clay and limestone debris – a detailed analysis will be presented later; such information allowed the authors to solve the ambiguity of the GPR interpretation. Due to the much lower resolution of the GCM method in comparison with the GPR method, in Figure 8 there is no possibility to distinguish between stochastically distributed fractures and more highly weathered parts of the limestone, like in Figure 5. In the GCM results, an additional anomaly in the initial part of the profiles over the cavern may be also distinguished (Fig. 8); this second potential anomalous zone was not confirmed by the results of the GPR surveys, therefore it was not analysed in the further parts of the section.

For the better visualisation of an anomalous zone visible in the central part of Figure 8, depth slices of 3D block were prepared (Fig. 9). In Figure 9, it is clearly visible that an anomalous zone is marked on all profiles; the shape, distribution and direction of the analysed anomaly is similar in both the GCM (Fig. 9) and the GPR (Fig. 6) results.

The results presented in Figures 8 and 9 and formerly in Figures 5–7 deliver spatial information which allows two general conclusions to be drawn: (a) limestone in the investigation site is divided by vertical discontinuities (faults?) into blocks, like in the horst structure, and (b) the areas between the blocks are filled by a mixture composed of clay material and debris made of fractured/weathered limestone.

Vertical blocks of limestone divided by zones made of the aforementioned mixture are clearly visible also in the x'-z plane (Fig. 10). Considering the electrical resistivity distribution shown in Figures 9 and 10, two types of anomalies can be distinguished:

- relatively high resistivity anomalies characterised by electrical resistivity values between 1,000 Ωm and over 2,500 Ωm; these anomalies are mainly marked at depths greater than 2 m and they are not continuous; these anomalies were interpreted as blocks of limestone;
- relatively low resistivity anomalies which are located mainly by the surface; they are characterised by resistivity values ranging between 100 Ωm and 250 Ωm and its thickness does not exceed 2 m; the same type of anomalies, divide high resistivity anomalies into blocks, were distinguished at depths greater than 2 m.

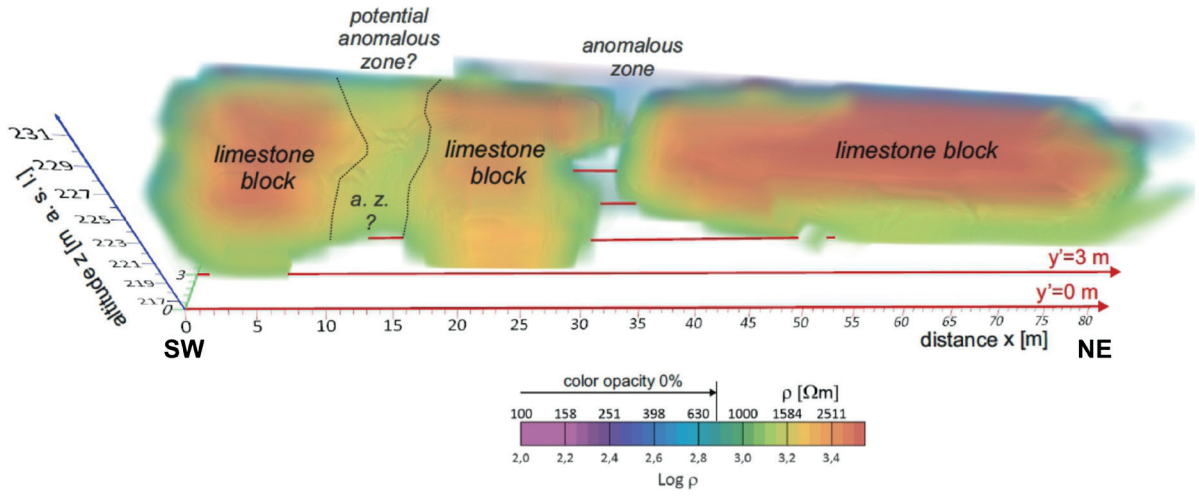

Fig. 8. *3D volumetric visualisation of the main GCM anomalies – a view from the rock mass towards surface*

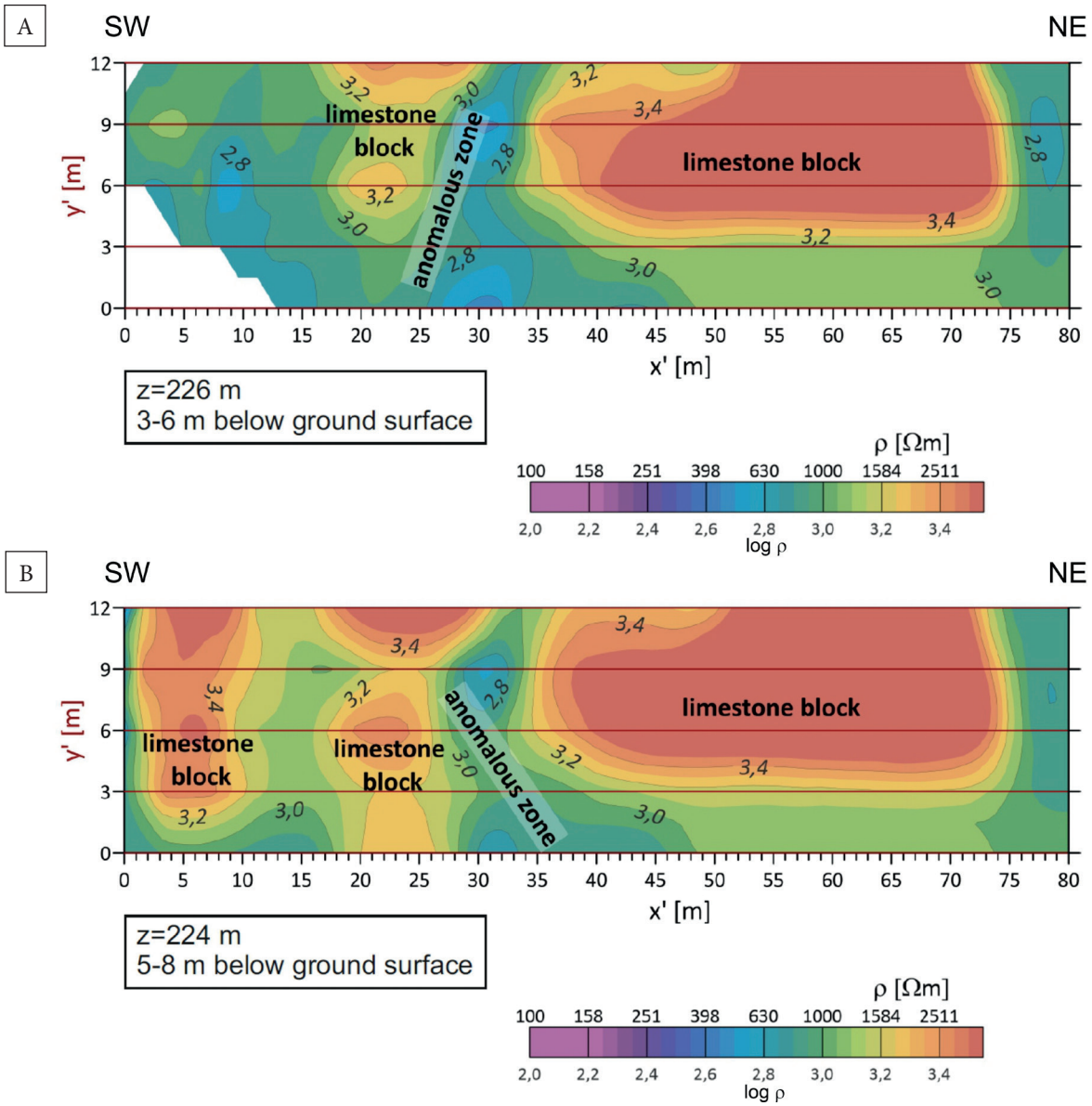

Fig. 9. *GCM results in form of depth slices of 3D block (Fig. 8) at: A) depth d = 5 m, altitude z = 226 m; B) depth d = 7 m, altitude z = 224 m*

Low resistivity anomalies indicate that we are not dealing with pure clay formations; in such a case, the electrical resistivity value is at most an order of magnitude too high (McNeill 1980). In such a setting, low resistivity anomalies should be interpreted rather as clay formation mixed with limestone rubble fragments than highly fractured/weathered limestone colmatated with clay material.

In order to check the geophysical interpretation, a shallow manual drilling (Fig. 11A) was made in the centre of and an anomalous zone. The site of the geophysical surveys was a private property, so we did not obtain permission for deep machine drilling. The geological material taken from the drillhole delivered the following information: between depths 0–0.5 m soil with small fragments of limestone was observed (Fig. 11B); between depths 0.5–1.0 m limestone debris with Quaternary material was revealed (Fig. 11C). Due to manual drilling, it was not possible to obtain geological material from greater depths

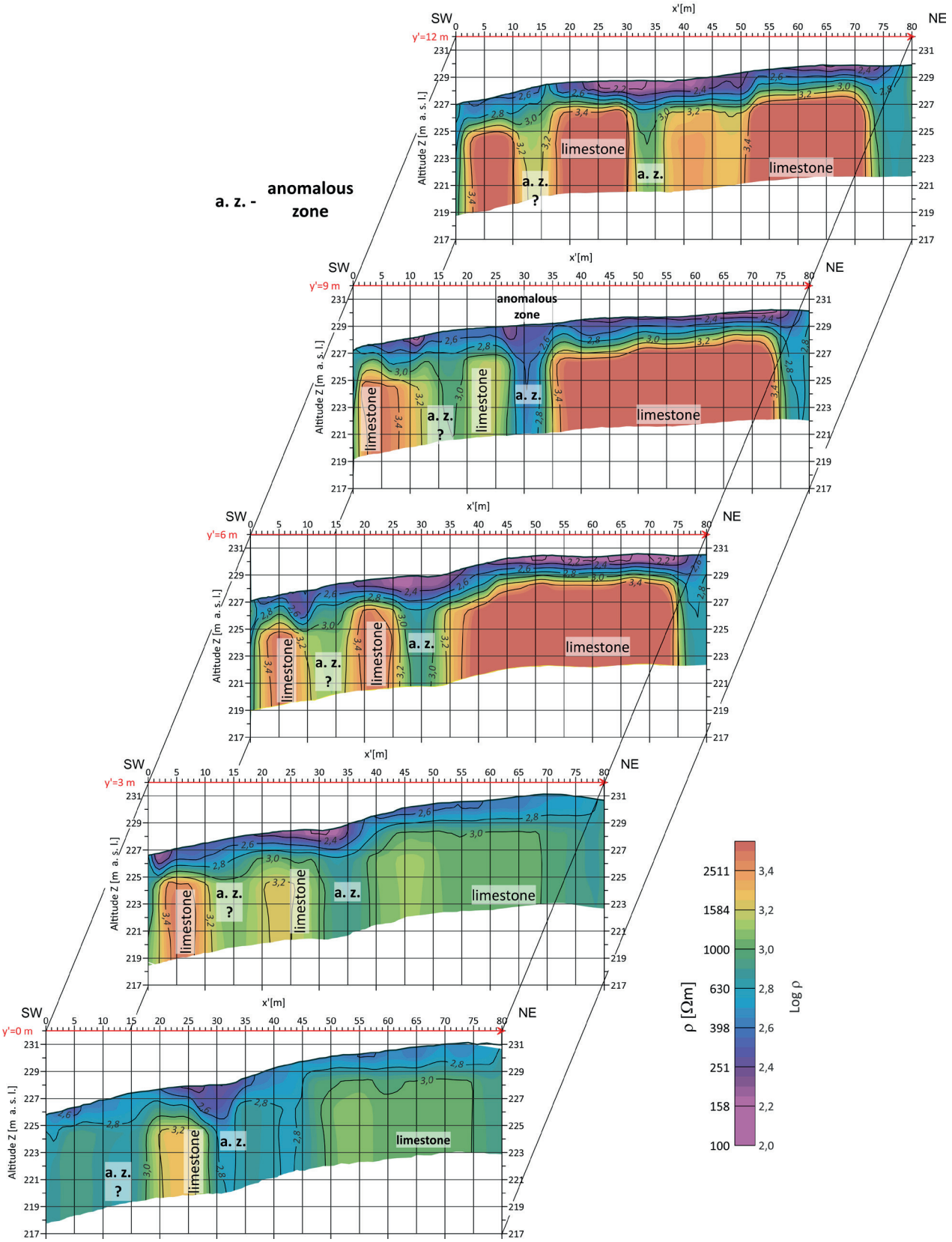

Fig. 10. *GCM results in form of y' cuts of 3D block (Fig. 8) with step Δy' = 3 m*

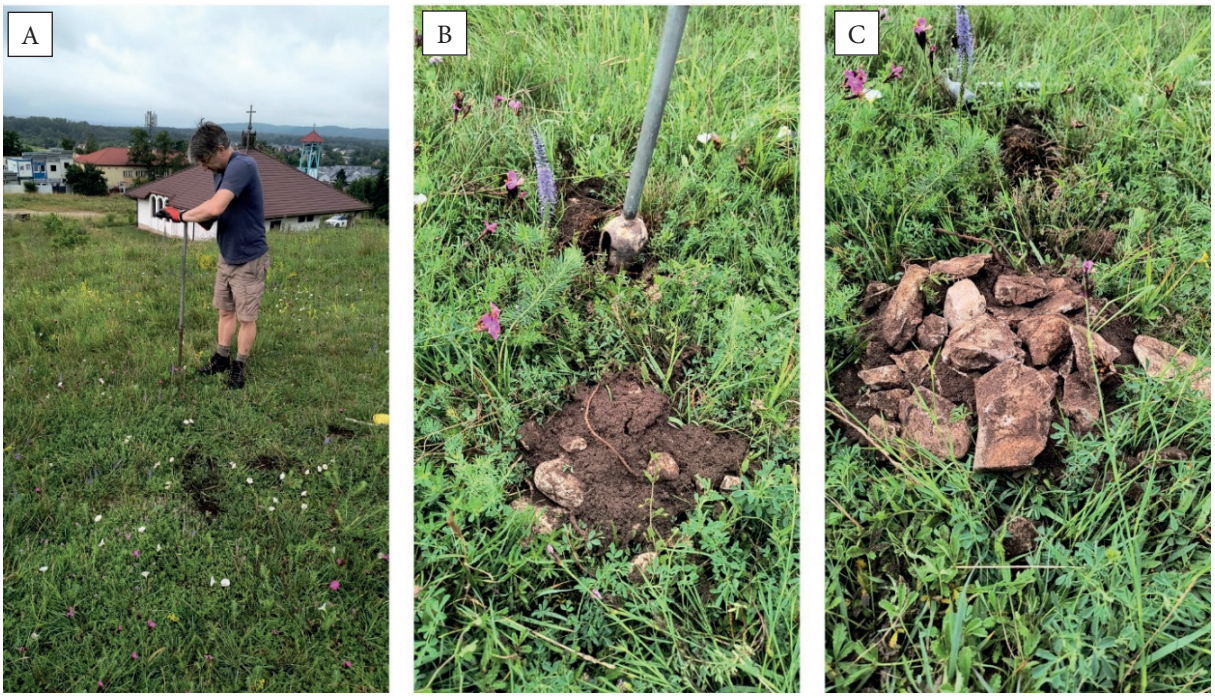

Fig. 11. *Verification drilling in the investigation site, named "The cavern under the chapel" (A); geological material taken from depths 0–0.5 m (B) and 0.5–1.0 m (C)*

"The Jasna cave" investigation site

The 3D volumetric visualisation of the main GPR anomalies in this site was prepared, but the 3D block was divided into four sub-blocks for the easier analysis of several anomalies (Fig. 12). For such a visualisation, amplitudes between several profiles were interpolated in the y' direction; afterwards, amplitudes were transformed into envelopes using the Hilbert transform; in the final step, an amplitude threshold was used; additionally, a shading procedure was applied to enhance the various anomalies.

In Figure 12 it may be seen that limestone is highly weathered/fractured in the near-surface zone, to depths of 10–15 m. Similarly to the first site, the scattering attenuation caused by such a zone did not strongly influence the GPR recordings from greater depths and in consequence several karst forms which had developed around the Jasna cave were detected.

In Figure 12A, apart from weathered/fractured zone, anastomoses (washouts between limestone beds) are also visible. An interesting anomaly is a kart chimney which developed in the initial parts of the profiles. Similarly to the first site, an anomalous zone characterised by the lack of reflections was recorded between $y' = 0$ m and $y' = 35$ m, and between $x' = 0$ m and $x' = 15$ m; this anomaly will be analysed in the further part of this sub-section.

In Figure 12Bit can be seen that a near-surface weathered/fractured zone is connected with fractures located at greater depths, so the thickness of the anomaly is higher. An anomalous zone without reflections may also be distinguished in this part of the rock mass.

Anomalies in Figure 12C have a fairly different distribution in comparison with Figure 12A, B. The weathered/fractured zone is thinner and four karst chimneys are visible here. An anomalous zone without reflections is still visible in this part of the investigation site.

An anomalous zone does not continue over the main chamber of the Jasna cave (Fig. 12D).

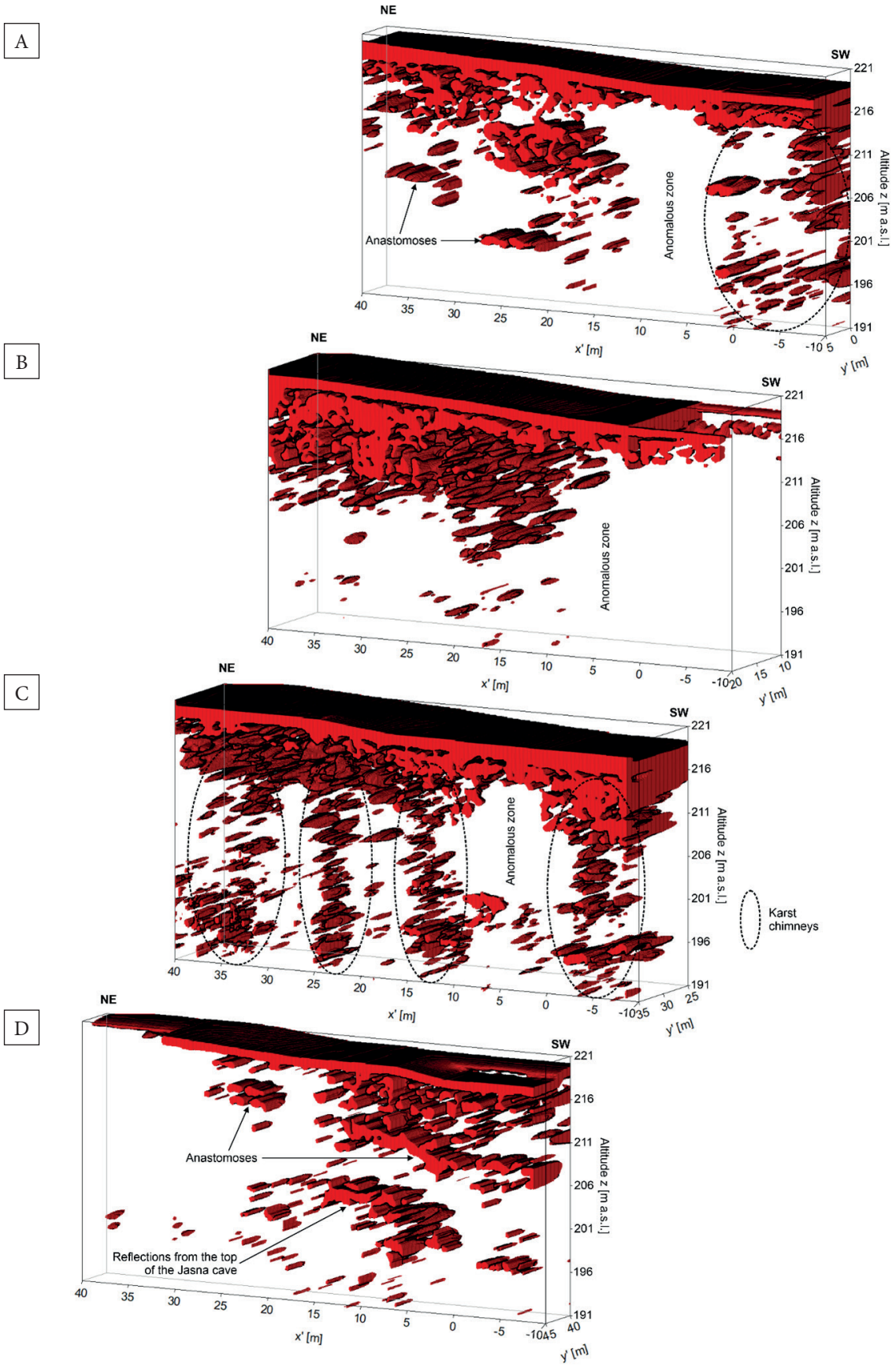

Fig. 12. *3D volumetric visualisation of the main GPR anomalies*

The profiles at $y' = 40$ m and $y' = 45$ m located directly over the main chamber of the Jasna cave (Fig. 3C) delivered the following information: the weathered/fractured zone is thin here, reflections from the main chamber are easily noticed and large anastomoses are revealed.

For the better analysis of the anomalous zone (where the reflections disappeared), depth slice and several x' cuts of 3D block were prepared (Fig. 13). Figure 13 was constructed by interpolation of information in the y′ direction and signal amplitudes were transformed into envelopes with the use of the Hilbert transform. An anomalous zone visible in Figure 13 has two interesting features:

- it appears suddenly, i.e. without any transition zone, in an area where karst forms (Fig. 12) and horst structure are well developed (Fig. 1B) – it may suggest that no vertical discontinuities (faults?) should exist in that place;
- it spreads vertically almost from the earth surface to the depth of approximately 30 m (Fig. 13B) – this effect is similar to that observed in the first site.

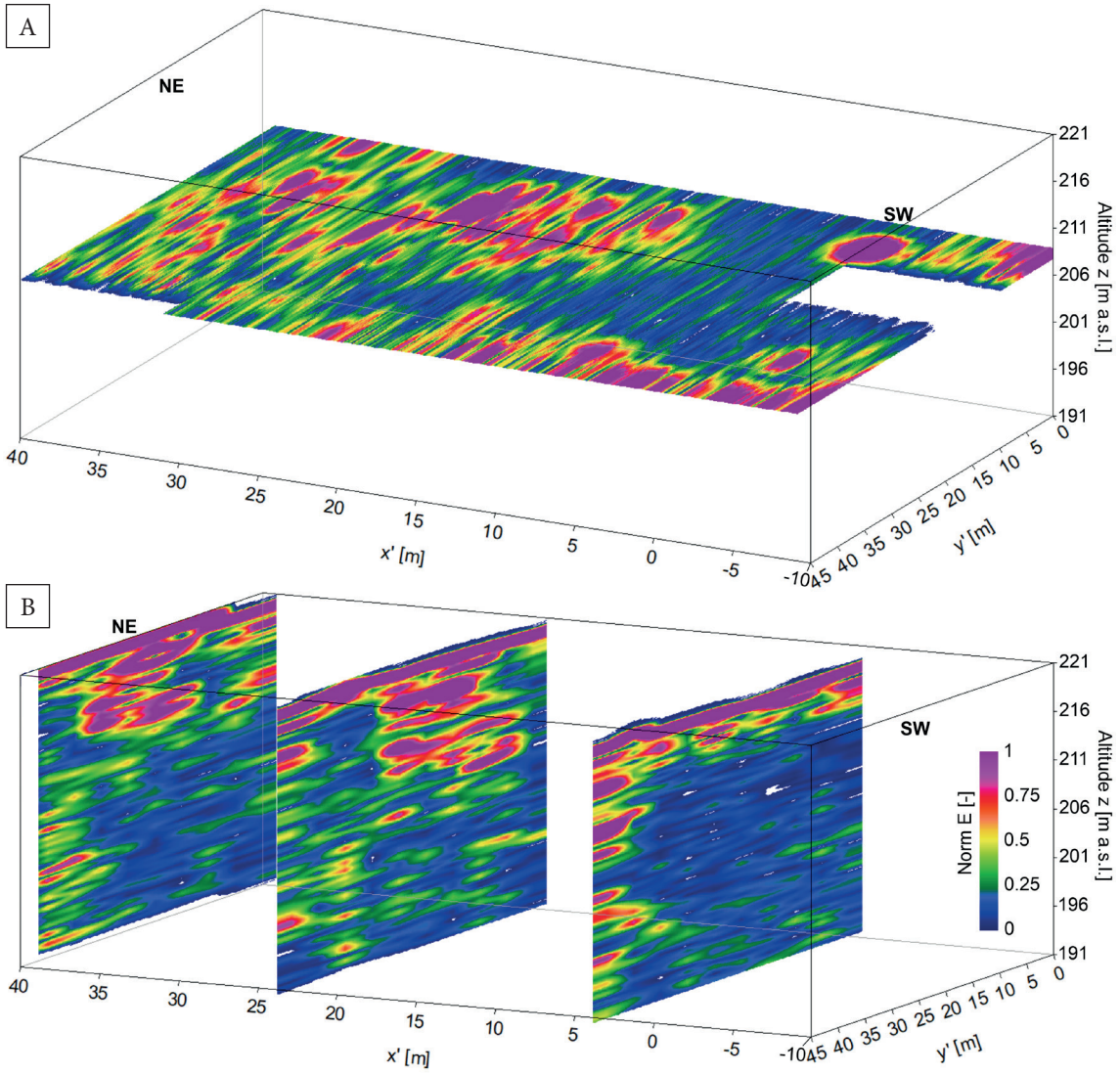

Fig. 13. *GPR results in form of several cuts: A) depth slice of 3D block (Fig. 12) at depth d = 13 m, altitude z = 208 m; B) x′ cuts of 3D block (Fig. 12) at x′ = 4 m (anomalous zone), x′ = 24 m, x′ = 40 m*

As mentioned earlier, the site of the geophysical surveys was a nature reserve, so there was no possibility of carrying out either manual or machine drilling to check the GPR interpretation. Therefore, the GPR results were correlated with the results obtained from another complementary, non-invasive method, i.e. ERT method. The ERT results were presented in paper by Pasierb (2022) and we referred to those results in this sub-section.

In Figure 14A, the 3D visualisation of the main ERT anomalies was presented; three high-resistivity anomalies, i.e. (1) – located around the cave (Fig. 14A, B), (2) and (3) may be distinguished; an additional anomaly with higher resistivity (4) was also recorded. Presence of high-resistivity anomalies in the studied area delivered information that free spaces were dry, i.e. filled with air, during the ERT surveys. It may be generally stated that the GPR and ERT results have lower consistency and similarity in comparison with the GPR and GCM results from the first site. This stemmed from the fact that that the terrain measurements over the Jasna cave were conducted during different weather conditions, a very important factor for electrical and electromagnetic methods. In this site, the profiles were similar but not the same – they have different orientations and lengths (Fig. 3C) which also influenced the final results.

The ERT anomaly (1) in Figure 14A, B may be correlated with several GPR anomalies recorded between $x' = -10$ m and $x' = 25$ m (Fig. 12D) and with three karst chimneys visible in the same area in Figure 12C.

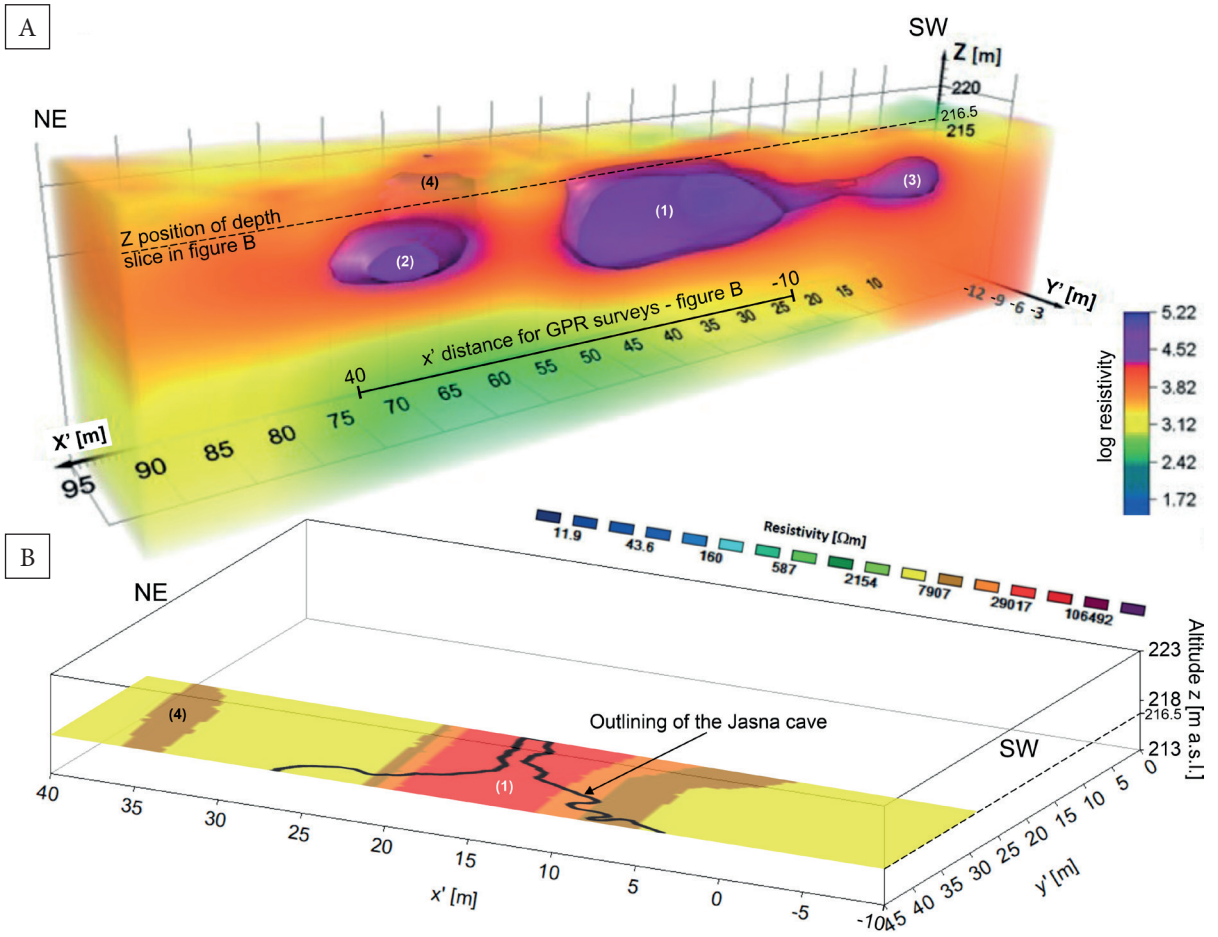

Fig. 14. *3D volumetric visualisation of the main ERT anomalies (Pasierb 2022 - modified) (A); depth slice of 3D block interpolated between depths of 6.0–6.5 m (Pasierb 2022 – modified) adjusted in coordinates to the GPR results (B)*

The ERT anomalies (2) and (4) may be correlated with a fourth karst chimney recorded from $x' = 30$ m to $x' = 40$ m (Fig. 12C). The resolution of the electrical measurements is low, therefore the results of ERT surveys delivered only a general outline of the GPR anomalies.

The ERT anomaly (3) is located beyond the region of the GPR surveys, so correlation is not possible.

Figure 14 delivered only general information, therefore the results obtained along the chosen ERT profiles should be analysed. For a more detailed interpretation, the measurements of the Jasna cave were introduced into the sub-section (Fig. 15).

The GPR and ERT profiles were located over the second part of the main chamber of the cave and over a small corridor (Fig. 15). There was no possibility of designing the geophysical profiles over the first part of chamber due to the presence of an escarpment in this site (Fig. 3B). Such a positioning of the profiles and the small dimensions of chamber and corridor under the investigation area meant that the effects originating from karst forms and horst structures should be recorded instead of those generated by the cave.

For a more detailed interpretation, the result obtained along profile ERT-2, located at $Y' = -4$ m, after 2D inversion (Fig. 16A) was put together with a radargram for the GPR profile designed at $y' = 40$ m (Fig. 16B). A Y' cut of 3D block (Fig. 14A), obtained from profiles ERT-4 (at $Y' = -12$ m) and ERT-5 (at $Y' = -16$ m), after 3D inversion was shown in Figure 16C; for comparison, a radargram for the GPR profile at $y' = 30$ m was presented in Figure 16D. In Figure 16 the main, high-resistivity ERT anomalies were inserted on radargrams; outlinines of the main, high-amplitude GPR anomalies were put on resistivity maps.

Taking into account the interpretation from the first site, for the analysis of the data recorded in the Jasna cave it was assumed that solid limestone has a resistivity 10^3 Ωm, a mixture of Quaternary deposits and limestone debris has resistivity 10^2 Ωm (in the further part of the text we use the abbreviation "mixture") and weathered/fractured rock mass has a resistivity 10^4–10^5 Ωm.

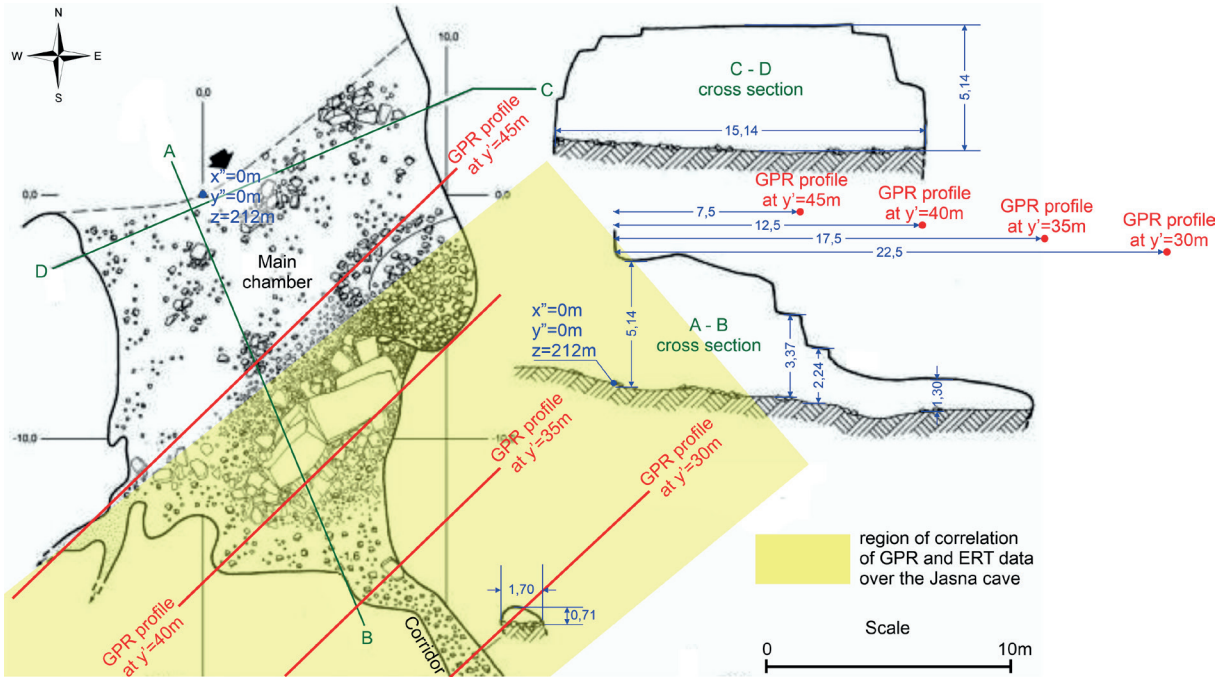

Fig. 15. *Measurements of geometry of the Jasna cave (https://jaskiniepolski.pgi.gov.pl/Details/Information/2082 – modified) in the region where correlation of GPR and ERT results was made*

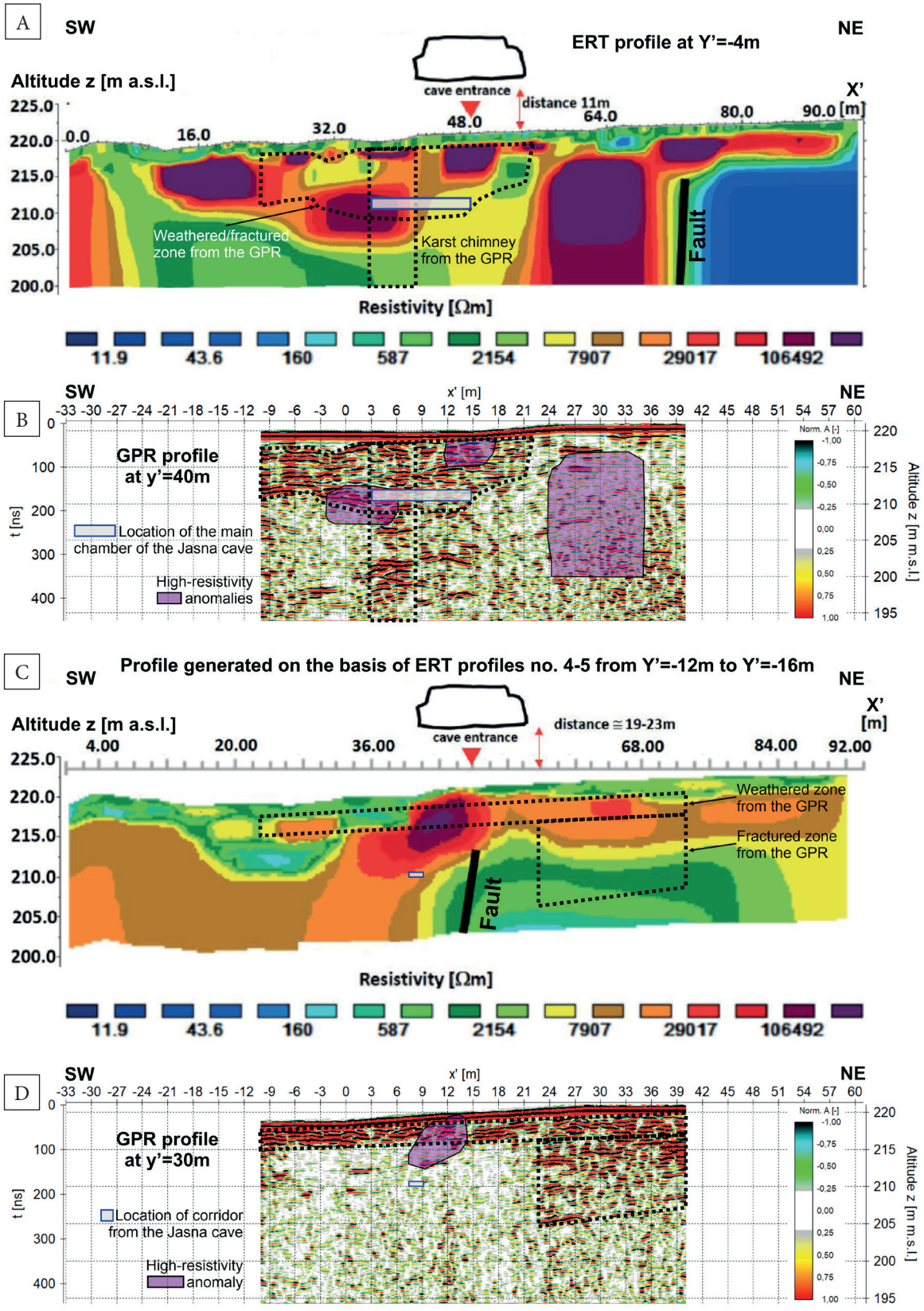

Fig. 16. *Cross-section along profile ERT-2, obtained from the 2D inversion (Pasierb 2022 – modified) (A); y' cuts of 3D block (Fig. 12 – GPR results) at y' = 40 m (B); cross-section along profiles ERT-4 and ERT-5 obtained from the 3D inversion (Pasierb 2022 – modified) (C); y' cuts of 3D block (Fig. 12 – GPR results) at y' = 30 m (D)*

Comparing the results of the ERT (Fig. 16A) and GPR (Fig. 16B) surveys, the following conclusions may be drawn:

- A vertical fault interpreted from the ERT data cannot be confirmed by the GPR results, due to the GPR profile being too short; assuming that the mentioned fault divides the investigation site into limestone blocks (Fig. 16A – X' from 0 m to 73 m) and areas filled with mixture (Fig. 16A – X' from 73 m to 92 m), the GPR results (Fig. 16B) were recorded entirely in limestone block.
- The karst chimney interpreted from the GPR data is partly confirmed by the presence of high-resistivity zones.
- The GPR anomaly caused by the presence of weathered and fractured zones is partly confirmed by a similar zone with higher resistivity; the shapes of both zones are similar, but in the ERT data the zone is shifted horizontally (due to the different locations and orientations of the GPR and ERT profiles) and has a slightly greater thickness.
- High-resistivity anomalies (overlayed on the radargram), depict the presence of a dry weathered zone (near the surface) and dry fractured zones (at greater depths) in the limestone blocks; two smaller ERT anomalies are located within a large high-amplitude GPR anomaly, but it is not possible to isolate any characteristic effects in these high-resistivity zones in the radargram; the largest high-resistivity anomaly is not confirmed by the GPR results.

Comparing the results of the ERT (Fig. 16C) and GPR (Fig. 16D) surveys, the following conclusions may be drawn:

- An almost vertical fault interpreted from the ERT data was not confirmed by the GPR results; assuming that the resistivity of limestone is ca. 10^3 Ωm, it seems that this fault is rather a boundary between solid limestone (higher resistivity) and fractured limestone (lower resistivity) where the free spaces are partly filled with water.
- The presence of two different parts of limestone was confirmed by the GPR results; the left part of rock mass, between $x' = -10$ m and $x' = 22$ m (Fig. 16D) may be interpreted as solid limestone, so no significant reflections were recorded here; in the right part of the rock mass, from $x' = 22$ m to $x' = 40$ m, high-amplitude reflections originated from fractures were recorded.
- The high-resistivity anomaly located over the corridor may be interpreted as dry weathered limestone; the GPR results only partly confirm the ERT anomaly, because on the radargram, a near-surface weathered zone has constat thickness equals ca. 3 m and spreads along the whole radargram.

In geophysics, final results depend strongly on: (a) project of terrain surveys and acquisition parameters, (b) numerous parameters assumed during data processing, (c) techniques of visualisation and (d) complex or individual interpretation. The GPR and ERT surveys over the Jasna cave were carried out by several teams, therefore at the stages of acquisition, processing, visualisation, and interpretation no consultation/cooperation was made, which caused the lower consistency and similarity of the results than in the first site.

CONCLUSIONS

Three-dimensional visualisation of the GPR data recorded in the site known as "the cavern under the chapel" allowed highly weathered and fractured limestone to be distinguished as existing up to a depth of approximately 10 m. Despite the existence of a 10-metre-thick zone with higher porosity, the scattering attenuation of such a zone did not disturb to record the reflections from the greater depths, i.e. from top of the cavern. An anomalous zone with highly reduced reflections' amplitudes was detected near the cavern. As discussed in the paper, such a GPR anomaly can be caused by at least two factors. The first may be due to the fact that there is a section of solid (i.e. unweathered/unfractured) limestone block at this location, and thus, the phenomenon of electromagnetic wave reflection should hardly occur. However, this hypothesis seems unlikely. A more realistic assumption was that in an anomalous zone weathered/fractured limestone was colmatated with Quaternary deposits, mainly with clay, and in consequence the ohmic attenuation caused the lack of reflections. The ambiguity

of the GPR interpretation was solved by using the GCM method. In the GCM results an anomalous zone also appeared in the same place as in the GPR results. The value of electrical resistivity in the anomalous zone, in the range of 600–1,000 Ωm, suggests rather the presence of fine limestone rubble mixed with Quaternary clay formations instead of weathered/fractured limestone colmatated with clay in this area. The complex geophysical interpretation was confirmed by shallow drilling which revealed a mixture composed of limestone debris and clay in the anomalous zone. The GCM results also allowed a block structure similar to a horst structure to be distinguished.

The 3D visualisation of the results of GPR surveys carried out in the second in the Jasna cave investigation site allowed a layer of highly weathered and fractured limestone existing up to the depth of approximately 10–15 m to be identified as in the first site. The thickness and distribution of this layer change markedly depending on the place in the research site which may suggest the presence of different limestone formations. The complex interpretation of the GPR and ERT data, carried out in 3D mode, allowed the visualisation and interpretation of additional karst forms besides of weathered/fractured zones, such as anastomoses and karst chimneys. In this site, an anomalous zone where reflections disappeared was also detected. In contrast to the first investigation site, the GPR anomalous zone here correlates with a region of increased resistivity in the ERT results, to value of 10^3 Ωm, which may indicate the presence of more solid limestone and, in consequence, the lack of conditions for the reflection of an electromagnetic wave. It is also worth mentioning that the higher-lying formations are characterised by a relatively lower resistivity by which the aforementioned resistivity value is better reflected by the inversion process. In the ERT results, two faults were interpreted. The first of them cannot be confirmed by the GPR results due to the profiles being too short. A comparison of the GPR and ERT results points to the fact that the second fault is rather a boundary between solid and fractured limestone. The investigation site over the Jasna cave is a reserve, so no verification drilling may be made in this site. The GPR and ERT results obtained have a lower consistency and similarity than the results from the first site. It was caused by the fact that terrain surveys, processing, visualisation and interpretation were conducted independently by two different teams and no cooperation on the mentioned stages of geophysical work was made. It is an important remark, for the further planning of complex geophysical investigations.

It is worth noting in closing that an important aspect limiting the ambiguity of interpretation was the supplementation of the GPR method with the other complementary GCM and ERT methods. In one of the research sites, verification drilling confirmed the complex geophysical interpretation. Karst forms and horst structures always have spatial and complicated geometry, so in our opinion only 3D visualisation of the geophysical surveys is the most appropriate.

The works were financed under the statutory activity of Department of Geoengineering and Water Management, Faculty of Environmental Engineering and Energy, Cracow University of Technology.

REFERENCES

Annan A.P., 1999. *Practical Processing of GPR Data*. Sensors and Software Inc., Ontario, Canada.

Annan A.P., 2001. *Ground Penetrating Radar*. Workshop Notes, Sensors and Software Inc., Ontario, Canada.

Armadillo E., Massa F., Caneva G., Gambetta M. & Bozzo E., 1998. Modeling of karst structures by geophysical methods. An example: the doline of S. Pietro dei Monti (Western Liguria). *Annali di Geofisica*, 41(3), 389–397. https://doi.org/10.4401/ag-4337.

Artugyan L., Ardelean A.C. & Urdea P., 2020. GPR and ERT Investigations of Karst Structures at the Buhui-Cuptoare Cave System, Anina Karst Region (Banat Mountains, Romania). [in:] Biswas A. & Sharma S. (eds.), *Advances in Modelling and Interpretation in Near Surface Geophysics*, Springer Geophysics, Springer, Cham, 19–38. https://doi.org/10.1007/978-3-030-28909-6_2.

Bozzo E., Lombardo S. & Metlanti F., 1996. Geophysical studies applied to near-surface karst structures: the dolines. *Annali di Geofisica*, 39(1), 23–38. https://doi.org/10.4401/ag-3948.

Everett M.E., 2013. *Near-Surface Applied Geophysics*. Cambridge University Press, Cambridge, UK.

Gołębiowski T., 2010. 3D GPR measurements for fractures detection in selected post-mining regions in Poland. [in:] *Near Surface 2010 – 16th EAGE European Meeting of Environmental and Engineering Geophysics: Zurich, Switzerland, 6–8 September 2010*, European Association of Geoscientists & Engineers, 728–732. https://doi.org/10.3997/2214-4609.20144911.

Gołębiowski T., 2012. *Zastosowanie metody georadarowej do detekcji i monitoringu obiektów o stochastycznym rozkładzie w ośrodku geologicznym*. Rozprawy, Monografie – Akademia Górniczo-Hutnicza im. Stanisława Staszica, 251, Wydawnictwa AGH, Kraków.

Gołębiowski T., 2023. Theoretical aspects and numerical modelling of the GPR method to analyse its possibilities for the detection of leakages in urban water supply networks. *Geology, Geophysics and Environment*, 49(4), 313–329. https://doi.org/10.7494/geol.2023.49.4.357.

Kasprzak M., Sobczyk A., Kostka S. & Haczek A., 2015. Surface geophysical surveys and LiDAR DTM analysis combined with underground cave mapping – an efficient tool for karst system exploration: Jaskinia Niedźwiedzia case study (Sudetes, SW Poland). [in:] Jasiewicz J., Zwoliński Z., Mitasova H. & Hengl T. (eds.), *Geomorphometry for Geosciences*, Bogucki Wydawnictwo Naukowe, Poznań, 75–79.

Leucci G., Margiotta S. & Negri S., 2004. Geophysical and geological investigations in a karstic environment (Salice Salentino, Lecce, Italy). *Journal of Environmental and Engineering Geophysics*, 9(1), 25–34. https://doi.org/10.4133/JEEG9.1.25.

Loke M.H., 2011. *Tutorial: 2-D and 3-D electrical imaging surveys*. Geotomo Software, Malaysia.

Łyskowski M., Mazurek E. & Ziętek J., 2014. Ground Penetrating Radar investigation of limestone karst at the Odstrzelona Cave in Kowala, Świętokrzyskie Mountains, Poland. *Journal of Cave and Karst Studies*, 76(3), 184–190. https://doi.org/10.4311/2014EX0001.

McNeill J.D., 1980. *Electrical Conductivity of Soils and Rocks*. Geonics Limited, Ontario, Canada.

Margiotta S., Negri S., Parise M. & Quarta T.A., 2015. Sinkhole field above karst caves: Detection and analysis through integrated techniques. [in:] Lollino G., Manconi A., Guzzetti F., Culshaw M., Bobrowsky P. & Luino F. (eds.), *Engineering Geology for Society and Territory – Volume 5: Urban Geology, Sustainable Planning and Landscape Exploitation*, Springer, Cham, 553–557. https://doi.org/10.1007/978-3-319-09048-1_107.

Martínez-Moreno F.J., Galindo-Zaldívar J., Pedrera A., Teixido T., Ruano P., Pena J.A., González-Castillo L., Ruiz-Constán A., López-Chicano M. & Martín-Rosales W., 2014. Integrated geophysical methods for studying the karst system of Gruta de las Maravillas (Aracena, Southwest Spain). *Journal of Applied Geophysics*, 107, 149–162. https://doi.org/10.1016/j.jappgeo.2014.05.021.

Maślakowski M., Lejzerowicz A., Pacanowski G. & Kuszyk R., 2024. The use of non-invasive ERT method to diagnose karst in roadengineering in the Lublin Upland. *Archives of Civil Engineering*, 70(1), 557–570. https://doi.org/10.24425/ace.2024.148928.

Motyka J., Czop M. & Polak K., 2003. Wpływ warunków wodnych w kamieniołomie „Zakrzówek" w Krakowie na jego funkcję rekreacyjną. [in:] Środulska-Wielgus J., Wielgus K. & Panek R. (red.), *Kształtowanie krajobrazu terenów poeksploatacyjnych w górnictwie: międzynarodowa konferencja naukowa: Kraków, 10, 11, 12 grudnia 2003 r.*, Biuro Usług Komputerowych Stanisław Smaga, Dębica, 208–219.

Ortyl Ł., 2019. Geometryzacja form zjawisk krasowych na podstawie badań metodą georadarową. *Przegląd Geologiczny*, 67(4), 252–269. https://doi.org/10.7306/2019.23.

Parczeński K., 2012. *Obrazowanie zjawisk krasowych przy pomocy metody GPR*. Cracow University of Science and Technology [Bachelor's degree thesis, supervisor T. Gołębiowski].

Pasierb B., 2022. The application of the 2D/3D electrical resistivity tomography (ERT) method in investigating the carbonate karst of the Zakrzówek Horst. *Geology, Geophysics and Environment*, 48(3), 319–327. https://doi.org/10.7494/geol.2022.48.3.319.

ReflexW Manual, 2023. *Sandmeier Geophysical Research*. Germany.

Reynolds J.M., 2011. *An Introduction to Applied and Environmental Geophysics*. 2nd ed. Wiley-Blackwell, Chichester.

Stan-Kłeczek I., Pierwoła J., Marciniak A., Sutkowska K., Tomaszewska R., 2022. Multimethod geophysical investigation in karst areas: Case studies from Silesia, Poland. *Bulletin of Engineering Geology and the Environment*, 81(6), 230. https://doi.org/10.1007/s10064-022-02726-8.

Trybuch G., 2024. *Wizualizacja 2D/3D/4D wyników badań geofizycznych prowadzonych dla wybranych zagadnień hydrogeologicznych* [*2D/3D/4D visualisation of geophysical data for selected hydrogeological problems*] [Bachelor's degree thesis, supervisor T. Gołębiowski].

Turarova M.K., Mirgalikyzy T., Mukanova B. & Modin I.N., 2022. Elimination of the ground surface topographic effect in the 2D inversion results of electrical resistivity tomography data. *Eurasian Journal of Mathematical and Computer Applications*, 10(3), 84–104. https://doi.org/10.32523/2306-6172-2022-10-3-84-104.

Verdet C., Sirieix C., Marache A., Riss J. & Portais J.C., 2020. Detection of undercover karst features by geophysics (ERT) Lascaux cave hill. *Geomorphology*, 360, 107177. https://doi.org/10.1016/j.geomorph.2020.107177.

Zieliński A., Mazurkiewicz E. & Łyskowski M., 2016. GPR mapping of karst formations under a historic building in Szydłów, Poland. *Geofizika*, 33(1), 101–111. https://doi.org/10.15233/gfz.2016.33.4.